Unstable mixed convection in an inclined porous channel with uniform wall heat flux

***A. Barletta[1], and M. Celli[1]**

[1]Department of Industrial Engineering, Alma Mater Studiorum Università di Bologna,
Viale Risorgimento 2, 40136 Bologna, Italy

*Corresponding author: antonio.barletta@unibo.it

Abstract

The aim of this paper is to analyse the onset of convective instability in a plane porous channel inclined to the horizontal. A net upslope or downslope flow is considered, so that mixed convection takes place as caused by the uniform and symmetric heat fluxes prescribed on the impermeable bounding walls. The thermoconvective instability of the basic flow is studied versus small-amplitude wavelike perturbations. The hybrid analytical-numerical technique adopted in this paper, in order to track and illustrate the parametric changes of neutral stability curves, is Galerkin's method of weighted residuals. Numerical values at significant points on the neutral stability curves are obtained by employing an accurate Runge-Kutta solver combined with the shooting method.

Keywords: Porous Medium, Convective Instability, Mixed Convection, Normal Modes

Introduction

Convective instability induced by thermal gradients is a subject widely explored in the literature. The typical setup giving rise to unstable behaviour is one where the vertical temperature gradient is directed downward. Such a configuration may pertain to a motionless basic state, as in the classical Rayleigh-Bénard problem and its many variants [Drazin and Reid (2004)], as well as to basic forced or mixed convection flow states.

A wide research work has been done over the last sixty years to investigate thermal instability in fluid saturated porous media. Surveys of the present knowledge in this field have been written by [Nield and Bejan (2013)], as well as by [Rees (2000)], by [Tyvand (2002)] and more recently by [Barletta (2011)]. Thermoconvective instability of a basic motionless state, much like as a porous medium version of the Rayleigh-Bénard problem, has been first studied by [Horton and Rogers (1945)] and [Lapwood (1948)]. These studies were relative to a horizontal layer with impermeable and isothermal walls kept at different temperatures, and they defined what is now well-known as the Darcy-Bénard problem.

A direct extension of the Darcy-Bénard problem arises when the plane porous layer is inclined to the horizontal. The pioneering papers on this subject are [Bories and Combarnous (1973)] and [Weber (1975)]. Important developments were obtained more recently by [Rees and Bassom (2000)]. The main effect of the layer inclination is that the basic state cannot be motionless, but it is given by a stationary and parallel buoyant flow with a zero mass flow rate.

The aim of this paper is to go beyond the analysis of the Darcy-Bénard problem in an inclined porous channel by devising a setup where both walls are impermeable and symmetrically heated or

cooled. The analysis to be carried out is an extension of what has been done by [Barletta (2012); (2013)], with reference to the special cases of a horizontal or vertical layer.

Mathematical model

Let us consider an inclined porous channel with infinite width and thickness H. The channel boundaries are the planes $z = 0, H$, tilted an angle $\phi \in [0, 90^\circ]$ to the horizontal (see Fig. 1). We will assume that these boundaries are impermeable and subject to symmetric wall heat fluxes, q_0. As the value of q_0 can be either positive or negative, this may result in either a net fluid heating or cooling, respectively.

Let us define the dimensionless quantities through the scaling

$$\begin{aligned} \text{coordinates:} \quad & (x,y,z)\,\frac{1}{H} \to (x,y,z), \\ \text{time:} \quad & t\,\frac{\varkappa}{\sigma H^2} \to t, \\ \text{velocity:} \quad & \boldsymbol{u} = (u,v,w)\,\frac{H}{\varkappa} \to (u,v,w) = \boldsymbol{u}, \\ \text{temperature:} \quad & \frac{T - T_0}{\Delta T} \to T, \end{aligned} \tag{1}$$

where T_0 is a reference constant temperature, and ΔT is a reference constant temperature difference defined as

$$\Delta T = \frac{q_0 H}{\lambda}, \tag{2}$$

while λ is the effective thermal conductivity, $\varkappa$ is the effective thermal diffusivity, and σ is the dimensionless ratio between the average heat capacity per unit volume of the porous medium and that of the fluid. Thus, according to the Oberbeck-Boussinesq approximation, and to Darcy's law for the momentum transfer in a porous medium, we may write the local balance equations of mass, momentum and energy in the dimensionless form

$$\boldsymbol{\nabla} \cdot \boldsymbol{u} = 0, \tag{3a}$$

$$\boldsymbol{\nabla} \times \boldsymbol{u} = R\,\boldsymbol{\nabla} \times \left[T\left(\sin\phi\;\hat{\boldsymbol{e}}_x + \cos\phi\;\hat{\boldsymbol{e}}_z\right)\right], \tag{3b}$$

$$\frac{\partial T}{\partial t} + \boldsymbol{u} \cdot \boldsymbol{\nabla} T = \nabla^2 T. \tag{3c}$$

Equation (3b) is obtained by evaluating the curl of both sides of the local momentum balance equation in order to encompass the dependence on the pressure field. The symbols $(\hat{\boldsymbol{e}}_x, \hat{\boldsymbol{e}}_y, \hat{\boldsymbol{e}}_z)$ denote the unit vectors along the $(x,y,z)-$axes, while the Darcy-Rayleigh number, R, is defined as

$$R = \frac{g\,\beta\,\Delta T\,K\,H}{\nu\,\varkappa}, \tag{4}$$

where g is the modulus of the gravitational acceleration $\boldsymbol{g}$, ν is the kinematic viscosity, and β is the thermal expansion coefficient of the fluid.

The boundary conditions are given by

$$\begin{aligned} z = 0: \quad & w = 0, \quad & \frac{\partial T}{\partial z} = -1, \\ z = 1: \quad & w = 0, \quad & \frac{\partial T}{\partial z} = 1. \end{aligned} \tag{5}$$

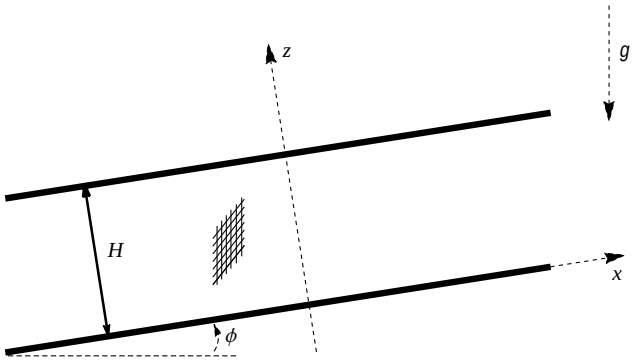

Figure 1. A sketch of the inclined porous layer

Basic solution

Equations (3) and (5) admit a time-independent basic solution expressed as

$$\begin{aligned} \boldsymbol{u}_b &= F(z)\,\hat{\boldsymbol{e}}_x, \\ \boldsymbol{\nabla} T_b &= \frac{2}{P}\,\hat{\boldsymbol{e}}_x + \frac{1}{P}\,G(z)\,\hat{\boldsymbol{e}}_z, \end{aligned} \tag{6}$$

where "b" stands for "basic solution", and

$$F(z) = \frac{\Omega}{2}\left[P\coth\left(\frac{\Omega}{2}\right) + 2\tanh\left(\frac{\Omega}{2}\right)\cot\phi\right]\cosh(\Omega z) - \frac{\Omega}{2}\,(P + 2\cot\phi)\sinh(\Omega z), \tag{7a}$$

$$G(z) = 2\cot\phi + \left[P\coth\left(\frac{\Omega}{2}\right) + 2\tanh\left(\frac{\Omega}{2}\right)\cot\phi\right]\sinh(\Omega z) - (P + 2\cot\phi)\cosh(\Omega z), \tag{7b}$$

while the parameter Ω is given by

$$\Omega = \sqrt{\frac{2R\sin\phi}{P}}, \tag{8}$$

and P is the Péclet number defining the average velocity in the porous channel,

$$P = \int_0^1 F(z)\,dz. \tag{9}$$

Equations (6) and (7) define a horizontal through flow in the $x-$direction, with a dimensionless flow rate given by P. Equation (6) reveals that this time-independent basic solution is possible only with a nonvanishing P. This feature reflects the obvious fact that, due to the heat flux either supplied ($R > 0$) or subtracted ($R < 0$) at both boundary walls, a stationary state is possible if and only if the net heat supplied/subtracted is convected along the channel.
From Eqs. (6)–(8), a symmetry of the basic solution is revealed, namely

$$\begin{cases} z \to 1 - z \\ R \to -R \\ P \to -P \end{cases} \quad \Longrightarrow \quad \begin{cases} \boldsymbol{u}_b \to -\boldsymbol{u}_b \\ \boldsymbol{\nabla} T_b \to -\boldsymbol{\nabla} T_b \end{cases} . \tag{10}$$

As a consequence of this symmetry, it is not restrictive to consider fluid heating conditions ($R > 0$) with either upslope mean flow ($P > 0$) or downslope mean flow ($P < 0$).

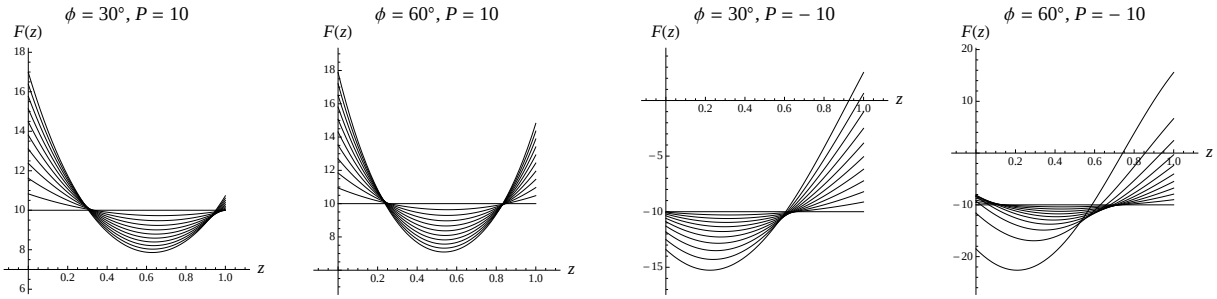

Figure 2. Plots of $F(z)$ for $P = \pm 10$, and $R = 0$ to 50 in steps of 5, with $\phi = 30^\circ$ and 60°

Eqs. (6)–(8) tend to the basic solution found by [Barletta (2012)] in the case of a horizontal channel ($\phi = 0^\circ$) with the same boundary conditions.

Fig. 2 illustrates, for $\phi = 30^\circ$ and 60°, how the uniform velocity profiles with $R = 0$ and $P = \pm 10$ are continuously deformed as R increases up to 50, in steps of 5. A phenomenon of flow reversal is evidenced in Fig. 2 when $P = -10$ and R becomes sufficiently high.

Linear stability analysis

Let us consider small-amplitude perturbations of the basic state,

$$\boldsymbol{u} = \boldsymbol{u}_b + \varepsilon \boldsymbol{U}, \qquad T = T_b + \varepsilon \Theta, \tag{11}$$

where ε is a perturbation parameter, $\varepsilon \ll 1$, and $\boldsymbol{U} = (U, V, W)$.

Substitution of Eq. (11) in Eqs. (3) and (5), by taking into account Eqs. (6)–(8), neglecting terms $\mathrm{O}(\varepsilon^2)$, and introducing an auxiliary scalar field Ψ such that

$$\boldsymbol{U} = R\left[\Theta\left(\sin\phi\ \hat{\boldsymbol{e}}_x + \cos\phi\ \hat{\boldsymbol{e}}_z\right)\right] - \boldsymbol{\nabla}\Psi, \tag{12}$$

yields

$$\nabla^2\Psi = R\left(\sin\phi\ \frac{\partial\Theta}{\partial x} + \cos\phi\ \frac{\partial\Theta}{\partial z}\right), \tag{13a}$$

$$\nabla^2\Theta = \frac{\partial\Theta}{\partial t} + F(z)\ \frac{\partial\Theta}{\partial x} + \frac{2}{P}\left(R\Theta\sin\phi - \frac{\partial\Psi}{\partial x}\right) + \frac{1}{P}\,G(z)\left(R\Theta\cos\phi - \frac{\partial\Psi}{\partial z}\right), \tag{13b}$$

$$z = 0, 1: \qquad \frac{\partial\Psi}{\partial z} = R\Theta\cos\phi, \qquad \frac{\partial\Theta}{\partial z} = 0. \tag{13c}$$

Normal mode analysis

We rely on the conclusion, drawn for the case $\phi = 0^\circ$ (horizontal channel) and for the case $\phi = 90^\circ$ (vertical channel) in [Barletta (2012); (2013)], to reckon that non-oscillatory longitudinal modes are the most unstable at onset. Thus, we will focus our stability analysis to these special normal modes,

$$\left\{\begin{array}{c}\Psi\\ \Theta\end{array}\right\} = \left\{\begin{array}{c}\psi(z)\\ \theta(z)\end{array}\right\}\exp\left[i(ky - \omega t)\right], \tag{14}$$

where k is the real-valued wave number, and ω is the complex-valued frequency. The real part of ω vanishes for non-oscillatory modes. The imaginary part of ω is the exponential growth parameter.

If $\mathrm{Im}(\omega) < 0$, the normal mode describes a stability condition. On the other hand, if $\mathrm{Im}(\omega) > 0$, the normal mode yields instability. In the following, we will be interested in the marginal stability condition, so that we will assume $\mathrm{Im}(\omega) = 0$.
By defining the new functions,

$$f(z) = \psi'(z) - R\,\theta(z)\cos\phi, \qquad h(z) = k\,\theta(z), \tag{15}$$

and substituting Eq. (14) into Eqs. (13), we obtain the linear stability eigenvalue problem, namely

$$f'' - k^2 f - Rkh\cos\phi = 0, \tag{16a}$$

$$h'' - \left(k^2 + \frac{2R}{P}\sin\phi\right)h + \frac{k}{P}\,G(z)\,f = 0, \tag{16b}$$

$$z = 0,1: \qquad f = 0, \qquad h' = 0. \tag{16c}$$

In Eqs. (15) and (16), the primes denote derivatives with respect to z.

Limiting case $|P| \gg 1$

When the Péclet number is very large we obtain a dramatic simplification of Eqs. (16). In fact, on account of Eq. (7b), we may approximate

$$\frac{G(z)}{P} \approx -(1-2z) + \mathrm{O}(P^{-1}). \tag{17}$$

Thus, when $P \gg 1$, Eqs. (16) assume the asymptotic form

$$f'' - k^2 f - Rkh\cos\phi = 0, \tag{18a}$$

$$h'' - k^2 h - k(1-2z)f = 0, \tag{18b}$$

$$z = 0,1: \qquad f = 0, \qquad h' = 0. \tag{18c}$$

Eqs. (18) allow us to infer that the neutral stability condition, expressed as $R\cos\phi$ versus k, is independent of the channel inclination angle ϕ. In other words, the inclination angle influences the neutral stability condition merely by rescaling $R(k)$, as obtained for a horizontal channel, with a factor $1/\cos\phi$. The immediate consequence of this behaviour is that a gradually increasing inclination has a stabilising effect. In fact, this conclusion applies in the asymptotic regime $|P| \gg 1$, while things are more complicated for finite values of $|P|$ as we will discuss in the next sections.

Method of weighted residuals

Equations (16) can be solved by expressing f and h as,

$$f(z) = \sum_{n=1}^{N} f_n \varphi_n(z), \qquad h(z) = \sum_{n=1}^{N} h_n \chi_n(z), \tag{19}$$

where N is the truncation order, $\{f_n, h_n\}$ are complex coefficients, and the test functions $\{\varphi_n(z), \chi_n(z)\}$ have to be chosen so that the boundary conditions Eq. (16c) are satisfied,

$$z = 0,1: \qquad \varphi_n = 0, \qquad \chi_n' = 0, \tag{20}$$

for every positive integer n. Normalised test functions are chosen, defined by

$$\varphi_n(z) = \sqrt{2}\sin[(n-1)\pi z], \qquad \chi_n(z) = \begin{cases} 1, & n = 1 \\ \sqrt{2}\cos[(n-1)\pi z], & n > 1 \end{cases} . \tag{21}$$

Substitution of Eq. (19) into Eqs. (16a) and (16b) yields the residuals

$$\sum_{n=1}^{N} \left[f_n \varphi_n''(z) - k^2 f_n \varphi_n(z) - R k h_n \chi_n(z) \cos\phi \right] = E(z), \tag{22a}$$

$$\sum_{n=1}^{N} \left[h_n \chi_n''(z) - \left(k^2 + \frac{2R}{P} \sin\phi \right) h_n \chi_n(z) + \frac{k}{P} G(z) f_n \varphi_n(z) \right] = \tilde{E}(z). \tag{22b}$$

A set of $2N$ algebraic equations is obtained by imposing that the weighted residuals are zero. Here, we adopt Galerkin's method, *i.e.* we assume that the weight functions coincide with the test functions. Thus, we can write

$$\int_0^1 E(z)\varphi_n(z)\,dz = 0, \quad \int_0^1 \tilde{E}(z)\chi_n(z)\,dz = 0, \quad n = 1,\ 2,\ \ldots\ ,\ N. \tag{23}$$

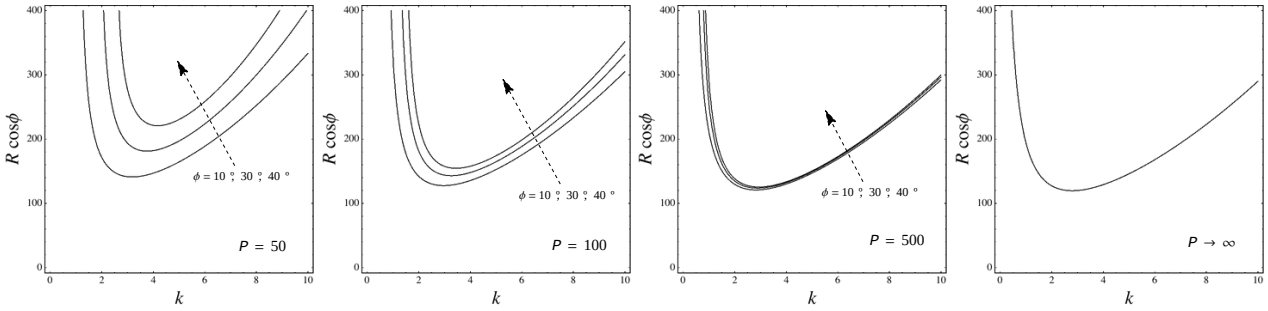

Figure 3. Neutral stability curves for $P = 50,\ 100,\ 500,\ \infty$, and $\phi = 10°$, $30°$ and $40°$

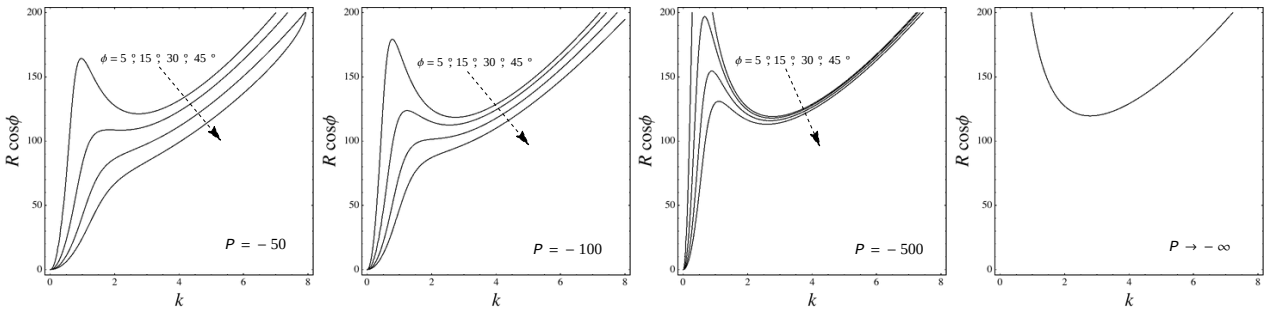

Figure 4. Neutral stability curves for $P = -50,\ -100,\ -500,\ -\infty$, and $\phi = 5°$, $15°$ $30°$ and $45°$

Eq. (23) can be rewritten in a matrix form as

$$\mathsf{M} \cdot \mathsf{c} = 0, \tag{24}$$

where M is a $2N \times 2N$ matrix and $\mathsf{c} = (f_1, f_2,\ \ldots\ , f_N, h_1, h_2,\ \ldots\ , h_N)$ is the vector of the expansion coefficients. Solving the eigenvalue problem (16) means determining non-vanishing vectors c satisfying Eq. (24), and this is accomplished when M has a vanishing determinant. Setting $\det(\mathsf{M}) = 0$

provides us with the neutral stability condition. This condition can be displayed graphically through plots of $R\cos\phi$ versus k, with prescribed values of (ϕ, P).

In Figs. 3 and 4, neutral stability curves in the $(k, R\cos\phi)$ plane are displayed, for either positive or negative Péclet numbers. Here, the computation has been carried out with a truncation order $N = 7$, which is sufficient for graphical purposes. Assessment of the solution method precision and of its convergence can be achieved by comparison with a highly accurate numerical solution based on a 4$^{\text{th}}$ order Runge-Kutta solver and on shooting method.

Numerical solution: combined Runge-Kutta method and shooting method

Another strategy for the solution of the eigenvalue problem (16) is achieved by combining use of an initial value ODE solver, *viz.* the 4$^{\text{th}}$ order Runge-Kutta method, with a technique employed to solve two-point problems, *viz.* the shooting method. This procedure is a standard approach in stability analyses. A survey can be found, for instance, in Chapter 9 of [Straughan (2010)].

The basic idea is to employ the 4$^{\text{th}}$ order Runge-Kutta method to solve Eqs. (16a) and (16b) with initial conditions based on an expanded form of the boundary conditions at $z = 0$ defined by Eq. (16c),

$$f(0) = 0, \quad f'(0) = \eta, \quad h(0) = 1, \quad h'(0) = 0. \tag{25}$$

Only the first and the last of these four initial conditions stem from Eq. (16c); the second one is just the definition of an unknown parameter η, while the third is a scale-fixing constraint for the eigenfunctions (f, h). In fact, the eigenfunctions are scale invariant due to the homogeneous nature of Eqs. (16), so that the setting $h(0) = 1$ can be invoked without any loss of generality. The parameter η, together with the eigenvalue $R\cos\phi$, is determined for every 3–tuple of input data (k, ϕ, P). Shooting method is employed for this task, with target constraints given by the boundary conditions at $z = 1$ and expressed by Eq. (16c), namely

$$f(1) = 0, \quad h'(1) = 0. \tag{26}$$

This procedure can be developed entirely within the *Mathematica 9* software environment (© Wolfram Research). Built-in functions `NDSolve` and `FindRoot` are the basic tools for implementing the 4$^{\text{th}}$ order Runge-Kutta solver, and the shooting method, respectively. This solution strategy is far more accurate than the method of weighted residuals described in the preceding section, but it requires longer computational times. Then, the method of weighted residuals is quicker and more effective for drawing plots of the neutral stability curves, while the present numerical method allows one to check its convergence and to determine accurate numerical data with given special parametric data (k, ϕ, P).

Table 1 reports the results of a convergence test for the eigenvalue $R\cos\phi$, with $\phi = 30^\circ$ and $k = 6$. The acronym MWR denotes method of weighted residuals, while RK4 stands for combined 4$^{\text{th}}$ order Runge-Kutta method and shooting method. While the latter method turns out to be accurate to more than six significant figures, the former is far less precise when $N \leq 8$. On the other hand, as $N > 8$, the computational time increases significantly. Overall, the agreement between the two methods is fairly satisfactory.

Discussion of the results and concluding remarks

The main features of the linear stability analysis can be inferred from inspection of Figs. 3 and 4. The effect of a gradually increasing inclination angle ϕ is dissimilar when P is either positive or negative. When $P > 0$, the effect of inclination is stabilising, as the neutral stability values of $R\cos\phi$ increase with the inclination angle ϕ. This feature reflects what we already noted in the discussion of the

Table 1. Convergence test for the eigenvalue $R\cos\phi$, with $\phi = 30^\circ$ and $k = 6$

Method	$P = -100$	$P = -50$	$P = 50$	$P = 100$
MWR ($N = 5$)	158.5	153.3	231.3	193.1
MWR ($N = 6$)	156.7	151.4	226.1	190.0
MWR ($N = 7$)	155.8	150.5	223.7	188.6
MWR ($N = 8$)	155.4	150.1	222.5	187.9
RK4	154.5902	149.3223	220.3801	186.5640

asymptotic case $|P| \gg 1$. When $P < 0$, even a small inclination to the horizontal may trigger the onset of instability, with a vanishingly small critical value of R. The instability is rather activated with small wave numbers, or large spatial wavelengths, as it is clearly evidenced in Fig. 4.

This behaviour implies a substantial reconsideration of the results obtained in the special case of a horizontal channel, as drawn by [Barletta (2012)]. In fact, when designing an experimental setup to test the flow stability in the horizontal case, a minimal misalignment in the channel inclination may have dramatic effects. Even a very small accidental inclination, with resulting downslope flow ($P < 0$), would imply instability. This is the case whatever small the wall heat flux and, hence, the value of R may be.

Finally, we note that the scaling law $R \sim 1/\cos\phi$, proved for the asymptotic case $|P| \gg 1$, does not hold when P is finite. Departure from this scaling law becomes more and more evident when $|P|$ is finite and decreases.

References

Barletta, A. (2011), Thermal instabilities in a fluid saturated porous medium. In Öchsner, A., Murch, G. E., editors, *Heat Transfer in Multi–Phase Materials*, pages 381–414. Springer, New York.

Barletta, A. (2012), Thermal instability in a horizontal porous channel with horizontal through flow and symmetric wall heat fluxes. *Transport in Porous Media*, **92**, 419–437.

Barletta, A. (2013), Instability of mixed convection in a vertical porous channel with uniform wall heat flux. *Physics of Fluids*, **25**, 084108.

Bories, S. A., Combarnous, M. A. (1973), Natural convection in a sloping porous layer. *Journal of Fluid Mechanics*, **57**, 63–79.

Drazin, P. G., Reid, W. H. (2004), *Hydrodynamic Stability*, 2nd edition. Cambridge University Press, New York, NY.

Horton, C. W., Rogers, F. T. (1945), Convection currents in a porous medium. *Journal of Applied Physics*, **16**, 367–370.

Lapwood, E. R. (1948), Convection of a fluid in a porous medium. *Proceedings of the Cambridge Philosophical Society*, **44**, 508–521.

Nield, D. A., Bejan, A. (2013), *Convection in Porous Media*, 4th edition. Springer, New York.

Rees, D. A. S. (2000), The stability of Darcy–Bénard convection. In Vafai, K., Hadim, H. A., editors, *Handbook of Porous Media*, chapter 12, pages 521–558. CRC Press, New York.

Rees, D. A. S., Bassom, A. P. (2000), Onset of Darcy–Bénard convection in an inclined layer heated from below. *Acta Mechanica*, **144**, 103–118.

Straughan, B. (2010), *Stability and Wave Motion in Porous Media*. Springer.

Tyvand, P. A. (2002), Onset of Rayleigh–Bénard convection in porous bodies. In Ingham, D. B., Pop, I., editors, *Transport Phenomena in Porous Media II*, chapter 4, pages 82–112. Pergamon, New York.

Weber, J. E. (1975), Thermal convection in a tilted porous layer. *International Journal of Heat and Mass Transfer*, **18**, 474–475.